Int. J. Electrochem. Sci., 13 **(2018)** 8506 – 8517, doi: 10.20964/2018.09.57

International Journal of
ELECTROCHEMICAL
SCIENCE
www.electrochemsci.org

Short Communication

Synthesis of Mo doped Ni_2S_3 nanaorods arrays for overall water splitting

Bin Liu[1*], *Xin-Yu Zhang*[1], *Tian-Shu Chen*[1], *Li-Ming Zhang*[1], *Xin-Lei Yang*[1], *Xue Ma*[1], *Di Liu*[2]

[1] State Key Laboratory of Heavy Oil Processing, College of Science, China University of Petroleum (East China), Qingdao 266580, PR China
[2] College of Chemical and Environmental Engineering, Shandong University of Science and Technology, Qingdao 266590, PR China
[*]E-mail: liubin@upc.edu.cn

Received: 7 May 2018 / *Accepted:* 5 July 2018 / *Published:* 5 August 2018

The development of stable and active electrocatalyst for both hydrogen evolution reaction (HER) and oxygen evolution reaction (OER) is of significant importance toward overall water splitting related with the conversion of sustainable energy sources. Herein, we report the synthesis of molybdate-directed Ni_3S_2 heterogeneous nanorod arrays, in which the nanorods decorated with vertical nanosheets were densely and evenly covered on the surface of Ni foam. Benefiting from the abundant accessible active sites, accelerated charge transport, fast release of generated gas, and synergistic effect, the Mo doped Ni_3S_2 nanorod arrays exhibits excellent activity toward both OER and HER, delivering current density of 100 $mA.cm^{-2}$ at low overpotential of 350 mV for OER and 290 mV for HER, respectively. Moreover, such heterogeneous nanorods display a very low cell voltage of 1.83 V to approach 100 $mA.cm^{-2}$ along with a favorable robustness for 10 h in an alkaline electrolyzer. Different characterizations including XRD and SEM revealed the influence of Mo doping on the growth of heterogeneous nanorods. Electrochemical measurements confirmed the superior activity of Mo doped Ni_3S_2 originated from synergistic effect of Mo and Ni_3S_2. This work sheds light on the fabrication of versatile electrocatalysts for efficient energy conversion by demonstrating the novel design of heterogeneous nanorods as active catalysts.

Keywords: Ni_3S_2; Mo doping; nanorod; electrocatalyst; overall water splitting

1. INTRODUCTION

The increasing environmental problems and rapid consumption on fossil fuels forced us to search for renewable and green energy alternatives to fossil fuels [1-3]. Water electrolysis, which were

combinated of the oxygen evolution reaction (OER) and hydrogen evolution reaction (HER), offering an alternative opportunity to generate oxygen and hydrogen, respectively [4-7]. The widespread implementation of electrochemical water splitting depends on innovative progress relating to the development of affordable and high-performance catalysts for hydrogen evolution reaction (HER) and oxygen evolution reaction (OER) [8-10]. Currently, the best electrocatalysts for HER and OER are Pt and RuO_2, respectively [11-15]. However, their large-scale availability is questionable due to the scarcity and consequent prohibitive cost. Therefore, substantial researches have been adopted to the exploration of promising alternative materials with favorable catalytic performance. For example, transition-metal chalcogenides, carbides and selenides including MoS_2 [16-18], CoS [19, 20], MoC_x [21], MnO_2 [22] and $CoSe_2$ [23], possesses stable HER activity in acidic media, while transition metal oxides/hydroxides including Co_3O_4/C [24, 25] and NiFe LDH [26], have shown favorable OER catalytic activity in alkaline electrolyte. Thus, for practical application, a bifunctional electrocatalyst is urgently required to concurrently catalyze the HER and OER under same electrolyte with high efficiency.

Benefited from synergistic effect of varied active sites and heterointerfaces, the construction of single heterogeneous nanostructure with HER and OER electrocatalysts provides a promise way for overall water splitting, in which they show superior performance than their single material counterparts towards both OER and HER [27-31]. That is, by combining OER and HER catalysts in rational designed way, they could be used as efficient bifunctional electrocatalyst. Such as, Nickle sulfides (e.g., Ni_3S_2, NiS_2), shown high activity as OER catalysts, but possess an unsatisfactory performance for overall water splitting due to its inferior HER activity [32-36]. Their HER activity and overall water splitting performance could be greatly improved by doping Mo into Nickle sulfides [37, 38]. Furthermore, to fulfill the synergistic effect of this heterogeneous nanostructure, it is highly necessary to construct a unique morphology, in which abundant active sites are fully manifested, charge transfer and gas release are greatly accelerated [39, 40]. In this regard, constructing Mo doped Ni_3S_2 electrocatalyst with unique nanostructures is an important step for efficient catalyze HER, OER and overall water splitting. Nevertheless, their fabrications are severely limited by demanding as well as complicated steps, in which always includes several surfactant-directed solvothermal procedures.

Herein, we demonstrate a facile molybdate-directed synthesis of heterogeneous Mo doped Ni_3S_2 nanorod arrays via environmental friendly hydrothermal process. Resulting from abundant activity sites as well as the synergetic effect between Mo and Ni_3S_2, this novel nanostructure shows enhanced catalytic activity, which achieves low overpotential of 290 and 350 mV at current density of 100 $mA.cm^{-2}$ for HER and OER, respectively. Moreover, when Mo doped Ni_3S_2 nanorod arrays served for catalyzing overall water splitting, it only affords a very low cell voltage of 1.83 V at current density of 100 $mA.cm^{-2}$ and remarkable robustness for successive 10 h of oxygen evolution. Additionally, the influence of molybdate for growth of nanostructures and enhanced catalytic performance has also been systematically investigated at varying molybdate content of 0, 20, 80, 100 mg. The mechanism and influence of molybdate to the nanostructure and performance of all materials are discussed in detail.

2. EXPERIMENTAL SECTION

2.1 Preparation of Ni_3S_2/NF, Mo-Ni_3S_2/NF-20, Mo-Ni_3S_2/NF-80 and Mo-Ni_3S_2/NF-100 nanorod arrays

All chemicals were bought from Aladdin Reagent and used without any further treatment. Mo-Ni-S/NF-100 nanorod arrays were fabricated through a one-step hydrothermal process. The preparation step is as follows: Nickle foam (NF, 1 cm × 2 cm) was successively cleaned by sonication in acetone, 0.5 M H_2SO_4, deionized water and ethanol for 30 min, respectively. 100 mg $(NH_4)_6Mo_7O_{24}\cdot 4H_2O$, 0.1 g P123, and 0.1 g CH_4N_2S were dissolved into 30 mL of DI water under magnetic stirring to form a clear solution. Four pieces of NFs and the obtained solution were transformed to a 100 mL Teflon-lined stainless steel autoclave and then kept for 24 h at constant 200°C. After it cooling down to nature temperature, the as-prepared NFs were washed by deionized water and ethanol for several times. Then the as-prepared NFs were dried at 60°C for 2 h in vacuum oven.

For comparison, the different contents of $(NH_4)_6Mo_7O_{24}\cdot 4H_2O$ (80 mg, 20 mg and 0 mg) were used to fabricate Mo-Ni-S/NF-80, Mo-Ni_3S_2/NF and Ni_3S_2/NF, respectively.

2.2 Physical characterization

X-ray diffraction patterns (XRD) were collected on X'Pert PRO MPD (Cu Kα1). The scanning electron microscopy (SEM) system (Hitachi, S-4800) was used to collect nanostructure of prepared materials. The X-ray photoelectron spectra (XPS; Thermo Fisher Scientific II) was conducted to study the oxidation states of main elements.

2.3 Electrochemical tests

The electrochemical tests were conducted in 1.0 M KOH solution by Gamry 600 electrochemical workstation on a classic three-electrode system. For OER measurement, saturated calomel reference electrode (SCE), Pt and as-prepared NFs were adopted as the reference electrode, counter electrode, and working electrode, respectively. The LSV were scanned between 0-0.7 V (vs. SCE) with a rate of 5 $mV.s^{-1}$. Cyclic voltammograms (CVs) were performed from 1.17 to 1.27 V (vs. RHE) by changing different scan rates (40, 60, 80, 100, and 120 $mV\cdot s^{-1}$), which could be used to evaluate the electrochemical double layer capacitances (Cdl) of all catalysts. The electrochemical spectroscopy (EIS) test was conducted at 1.53 V (vs. RHE) with the frequency range from 100 kHZ to 10^{-1} Hz. For HER measurement, the saturated calomel reference electrode (SCE), the graphite rod and the as-prepared NFs were adopted as the reference electrode, counter electrode, and working electrode, respectively. The polarization curves were scanned from -1–1.7 V (vs. SCE) with a rate of 5 $mV.s^{-1}$. Cyclic voltammograms (CVs) were performed from 0.17 to 0.27 V (vs. RHE) by changing different scan rates (40, 60, 80, 100, and 120 $mV\cdot s^{-1}$), which could be used to evaluate the electrochemical double layer capacitances (Cdl) of all catalysts. The electrochemical spectroscopy (EIS) test was conducted under -0.1 V (vs. RHE) with frequency range scanning from 100 kHZ to 10^{-1} Hz.

The bifunctional water splitting performance of Mo-Ni-S/NF-100 was carried on 1 M KOH, in which the Mo-Ni-S/NF-100 were adopted as both anode and cathode with a potential range scanning from 0-0.7 V (vs. RHE). The stability of Mo-Ni-S/NF-100 sample was evaluated via a long-term chronoamperometry with a constant potential at 1.81 V for 10 h.

3. RESULTS AND DISCUSSION

The crystallographic information of catalysts was examined by XRD, as displayed in Figure 1. It should be observed that 44.6°, 51.9° and 76.6° are ascribed to the NF substrate (PDF No.01-070-0989). The 21.8°, 31.2°, 37.9°, 49.9°, 55.5°, 65°, 73.3° and 78.1° diffractions peaks can be assigned to the (100), (1-10), (111), (210), (1-21), (2-20), (310) and (1-31) planes of Ni_3S_2, respectively (PDF No. 01-085-0775). For Mo-Ni_3S_2/NF-100 samples, the characteristic peaks of Mo_8O_{23} are detected at 35.9°, 40.9° and 54.5°, which can be ascribed to (412), (512) and (019) crystal planes, respectively (PDF No.01-084-1248). It is noteworthy that only weak diffraction peaks of Mo_8O_{23} can be observed in Mo-Ni_3S_2/NF-20 and Mo-Ni_3S_2/NF-80, due to the low doping content of $(NH_4)_6Mo_7O_{24}\cdot 4H_2O$ for synthesis process.

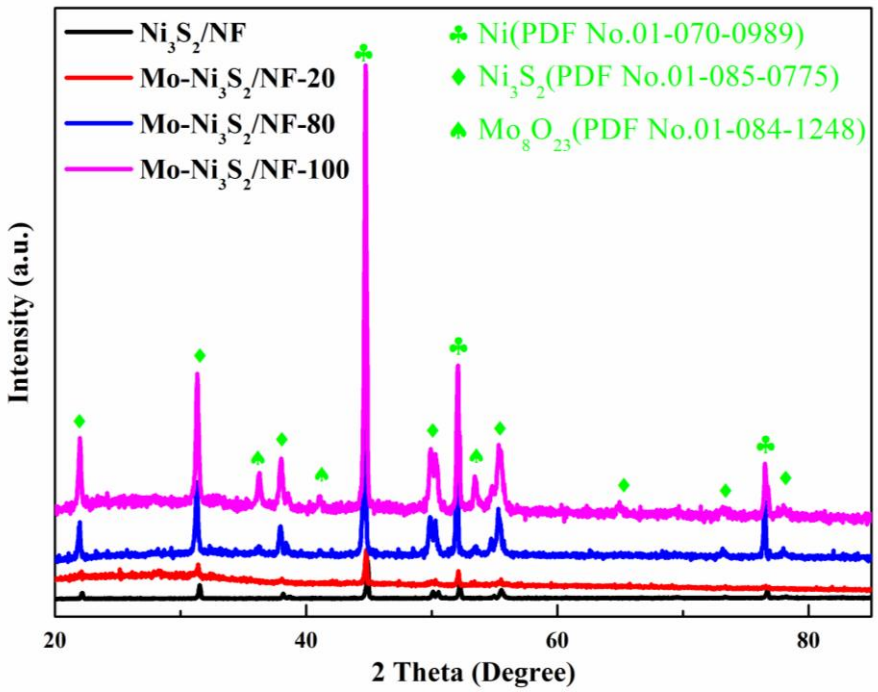

Figure 1. XRD patterns of Ni_3S_2/NF, Mo-Ni_3S_2/NF-20, Mo-Ni_3S_2/NF-80 and Mo-Ni_3S_2/NF-100

The surface valence states of dominant constituent elements were characterized by X-ray photoelectron spectroscopy (XPS) measurement. Mo-Ni_3S_2/NF-100 was selected as the aimed electrocatalyst because it shows best catalytic performances among all prepared comparison electrocatalysts (see detailed discussion below). As shown in Figure 2, the Mo-Ni_3S_2/NF-100 presents elements of Ni, S and Mo, indicating that Mo is successfully integrated into catalyst forming Mo

doped Ni_3S_2 heterogenous electrocatalyst. For Ni 2p region (Figure 2b), it clearly displays the obvious peaks at 855.2 eV and 873.2 eV for Ni $2p_{3/2}$ and $2p_{1/2}$, respectively. This was consistent with previously reported Ni species in Ni_3S_2 [41]. Meanwhile, the Mo-Ni_3S_2/NF-100 shown visible peaks for S $2p_{3/2}$ and S $2p_{1/2}$ at 162.5, 163.9 eV, respectively, indicating unsaturated S atoms on Ni-S (Figure 2c) [42, 43]. In addition, the Mo-Ni_3S_2/NF-100 also exhibited coincident binding energies for Mo^{6+} (Figure 2d) [42]. The existence of Mo^{6+} is due to the Mo_8O_{23} in Mo-Ni_3S_2/NF-100, which was coincident with the XRD result.

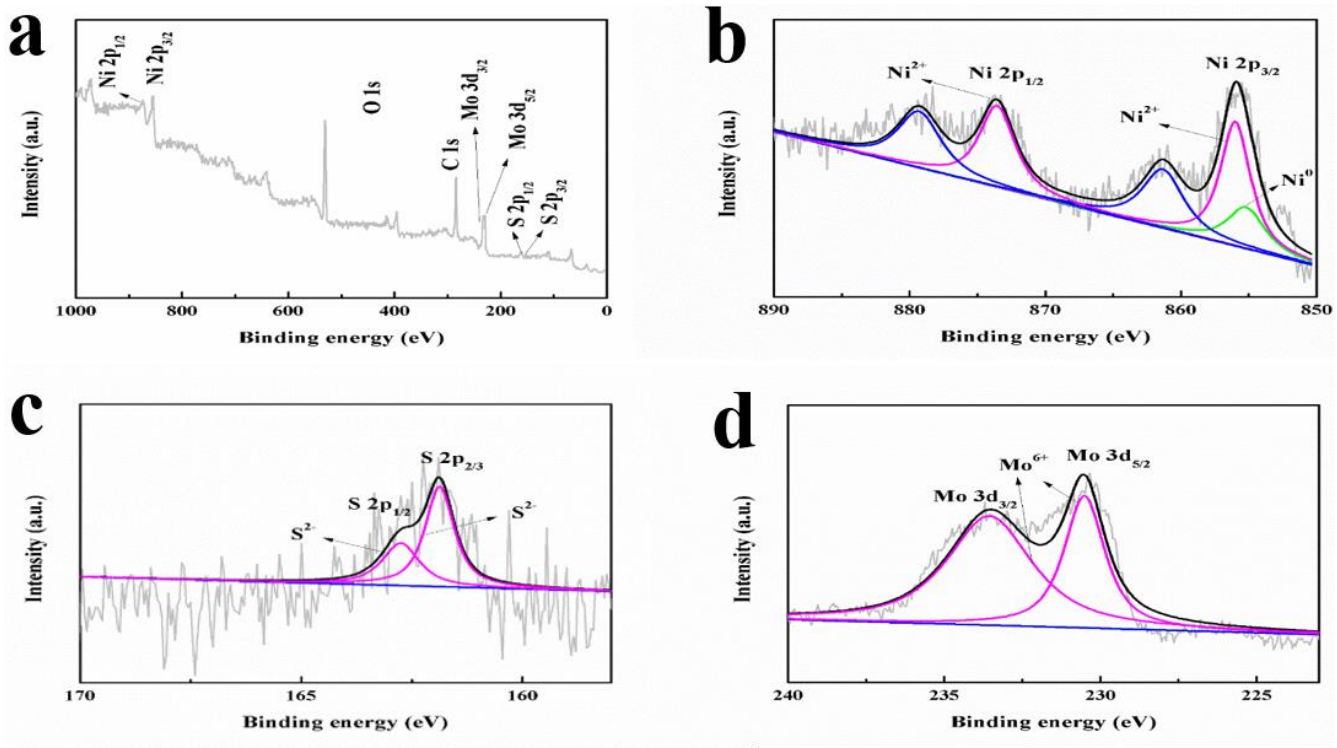

Figure 2. (a) XPS survey spectra for Mo-Ni_3S_2/NF-100 in the (b) Ni 2p; (c) S 2p and (d) Mo 3d regions

Figure 3 shows SEM images of Ni_3S_2/NF, Mo-Ni_3S_2/NF-20, Mo-Ni_3S_2/NF-80 and Mo-Ni_3S_2/NF-100. In general, the Ni_3S_2/NF presented ripple-like morphology (Figure 3a-b), while the Mo-Ni_3S_2/NF-20 presented bulge-like structures on the NF (Figure 3c-d), suggesting the doping of Mo could have significant influence on the morphologies of as-prepared samples. Meanwhile, as the content of Mo is increase to 80 mg, the whole surface of Ni surface was densely and uniformly covered with nanorods with diameters of 1 um. Besides, the surface of this unique nanorod consists of numerous decorated vertical-intersected nanosheets, implying accessibility of abundant active sites, accelerated charge transfer and fast diffusion of generated gas products. Similar nanorod arrays were also detected in Mo-Ni_3S_2/NF-100, resulting in superior catalytic activity of Mo-Ni_3S_2/NF-100. Therefore, these results strongly suggest the existence of molybdate beneficial for the growth of nanorod, which due to the anisotropic growth of molybdate anions [44, 45]. Moreover, such heterogeneous nanorod arrays with associated advantages of high surface area, synergistic effect of Mo and Ni_3S_2, and favorable conductivity will be a suitable choice for electrochemical reactions.

The OER activities of the Ni_3S_2/NF, Mo-Ni_3S_2/NF-20, Mo-Ni_3S_2/NF-80 and Mo-Ni_3S_2/NF-100 were first evaluated by linear scan voltammetry (LSV) with scan rate of 5 $mV.s^{-1}$ in 1 M KOH solution (Figure 4a). The Ni_3S_2/NF exhibited OER overpotential of approximately 520 mV to deliver current density of 50 $mA.cm^{-2}$. By contrast, the Mo-Ni_3S_2/NF-20, Mo-Ni_3S_2/NF-80 and Mo-Ni_3S_2/NF-100 demonstrate overpotentials of 470, 390 and 350 mV to afford current density of 100 $mA.cm^{-2}$, respectively. Thus, the overpotentials of these samples were greatly lowered with different degrees due to the doping of Mo.

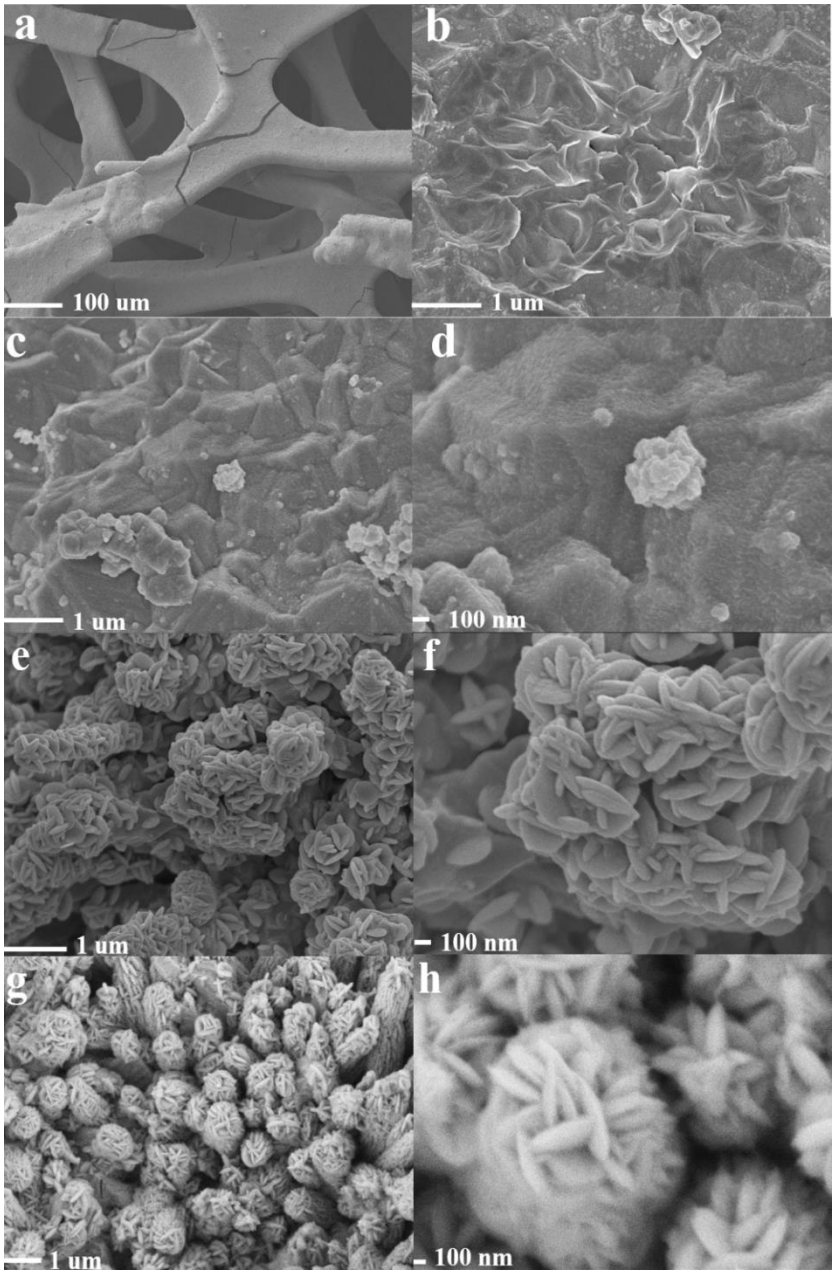

Figure 3. SEM images. (a,b) Ni_3S_2/NF (c,d) Mo-Ni_3S_2/NF-20 (e,f) Mo-Ni_3S_2/NF-80 and (g,h) Mo-Ni_3S_2/NF-100

The corresponding Tafel plots of Ni_3S_2/NF, Mo-Ni_3S_2/NF-20, Mo-Ni_3S_2/NF-80 and Mo-Ni_3S_2/NF-100 are 343.05, 242.96, 562.75 and 408.74 mV.dec^{-1}, respectively (Figure 4b). The obtained resistance results of HER and OER in 1 M KOH solution were further fitted by the Randles equivalent circuit. In the meantime, electrochemical impedance spectroscopy (EIS) (Figure 4c) shows the different charge-transfer resistance values of Ni_3S_2/NF, Mo-Ni_3S_2/NF-20, Mo-Ni_3S_2/NF-80, and Mo-Ni_3S_2/NF-100. Correspondingly with the order of OER performance, Mo-Ni_3S_2/NF-100 presents a significantly lower R_{ct} than those of Ni_3S_2/NF, Mo-Ni_3S_2/NF-20 and Mo-Ni_3S_2/NF-80. This result demonstrates that the fast electron transport of Mo-Ni_3S_2/NF-100 for oxygen generation on the nanorod arrays directly grown on conducting NF. As displayed in Figure 4d, the results of C_{dl} for Ni_3S_2/NF, Mo-Ni_3S_2/NF-20, Mo-Ni_3S_2/NF-80 and Mo-Ni_3S_2/NF-100 show consistent trends. Specifically, the Mo-Ni_3S_2/NF-100 with Mo doping of 100 mg possesses maximal C_{dl} of 33.34 mF.cm^{-2}. This clearly suggest the larger electrochemical active surface area and greater amounts of active sites achieved on Mo-Ni_3S_2/NF-100 for oxygen evolution.

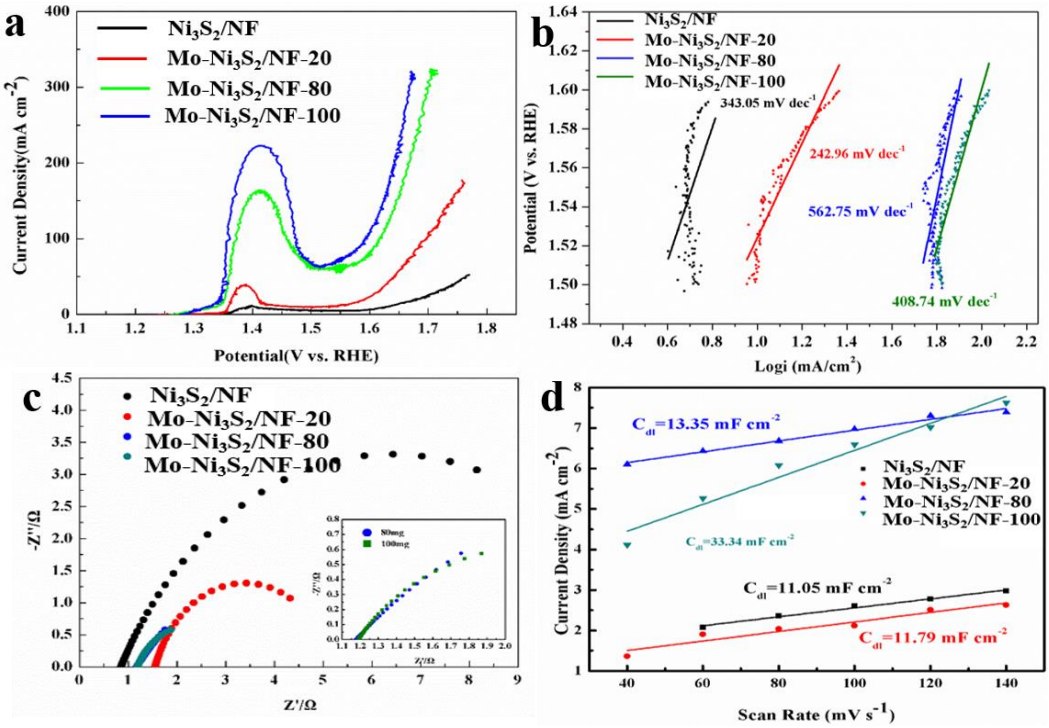

Figure 4. (a) Comparison of LSV curves on Ni_3S_2/NF, Mo-Ni_3S_2/NF-20, Mo-Ni_3S_2/NF-80 and Mo-Ni_3S_2/NF-100 for OER. (b) Corresponding Tafel plots extracted from panel a. (c) Nyquist plots of Ni_3S_2/NF, Mo-Ni_3S_2/NF-20, Mo-Ni_3S_2/NF-80 and Mo-Ni_3S_2/NF-100 at 1.53 V (vs. RHE) from 10^5 to 0.1 Hz. (d) C_{dl} values of Ni_3S_2/NF, Mo-Ni_3S_2/NF-20, Mo-Ni_3S_2/NF-80 and Mo-Ni_3S_2/NF-100.

The HER electrocatalytic performances of the above samples were also evaluated in 1 M KOH electrolyte. The LSV curve shown in Figure 5a, in which the applied overpotential of Ni_3S_2/NF to deliver 50 mA.cm^{-2} is approximately 0.35 V. To delivering current density of 100 mA.cm^{-2}, the Mo-Ni_3S_2/NF-20, Mo-Ni_3S_2/NF-80 and Mo-Ni_3S_2/NF-100 need overpotential of 0.37, 0.31 and 0.29 V,

respectively, suggesting the superior activity achieved on Mo-Ni_3S_2/NF-100 because of its optimal catalyst composition and large specific surface area. The Tafel slopes of Ni_3S_2/NF, Mo-Ni_3S_2/NF-20, Mo-Ni_3S_2/NF-80, and Mo-Ni_3S_2/NF-100 are 135.78, 145.99, 169.9 and 213.06 mV.dec^{-1}, respectively (Figure 5b). Similarly, charge-transfer resistances (Rct) are also important factor influencing HER process [46, 47]. The Mo-Ni_3S_2/NF-100 shows charge transfer resistance of 1.52 **Ω**, while the values for Ni_3S_2/NF, Mo-Ni_3S_2/NF-20 and Mo-Ni_3S_2/NF-80 were much higher. The enhanced electrical conductivities of Mo-Ni_3S_2/NF-100 could be attributed to the existence of nanorod arrays and optimal catalyst composition (Figure 5c). Since the electrochemically active surface area (ECSA) is a critical criterion for assessing active sites for catalysts, and the ECSA and the double-layer capacitances (C_{dl}) value has positive linear relationship [48-51]. Thus, varied scan rates (40, 60, 80, 100, 120 mV.s^{-1}) of cyclic voltammetry were performed in 1 M KOH solution to get the C_{dl}. As shown in Figure 5d, the C_{dl} of Ni_3S_2/NF and Mo-Ni_3S_2/NF-20 are 4.05 and 14.16 mF.cm^{-2}, respectively, lower that that of Mo-Ni_3S_2/NF-80 (16.80 mF.cm^{-2}) and Mo-Ni_3S_2/NF-100 (26.95 mF.cm^{-2}). The result is associated with their unique nanorod arrays, indicating more active sites, and thus enhanced OER performance of Mo-Ni_3S_2/NF-80 and Mo-Ni_3S_2/NF-100. Furthermore, compared with Mo-Ni_3S_2/NF-80, as increase of Mo doping, the improved active surface area on Mo-Ni_3S_2/NF-100 is due to optimal catalyst composition originated from the increase of Mo doping.

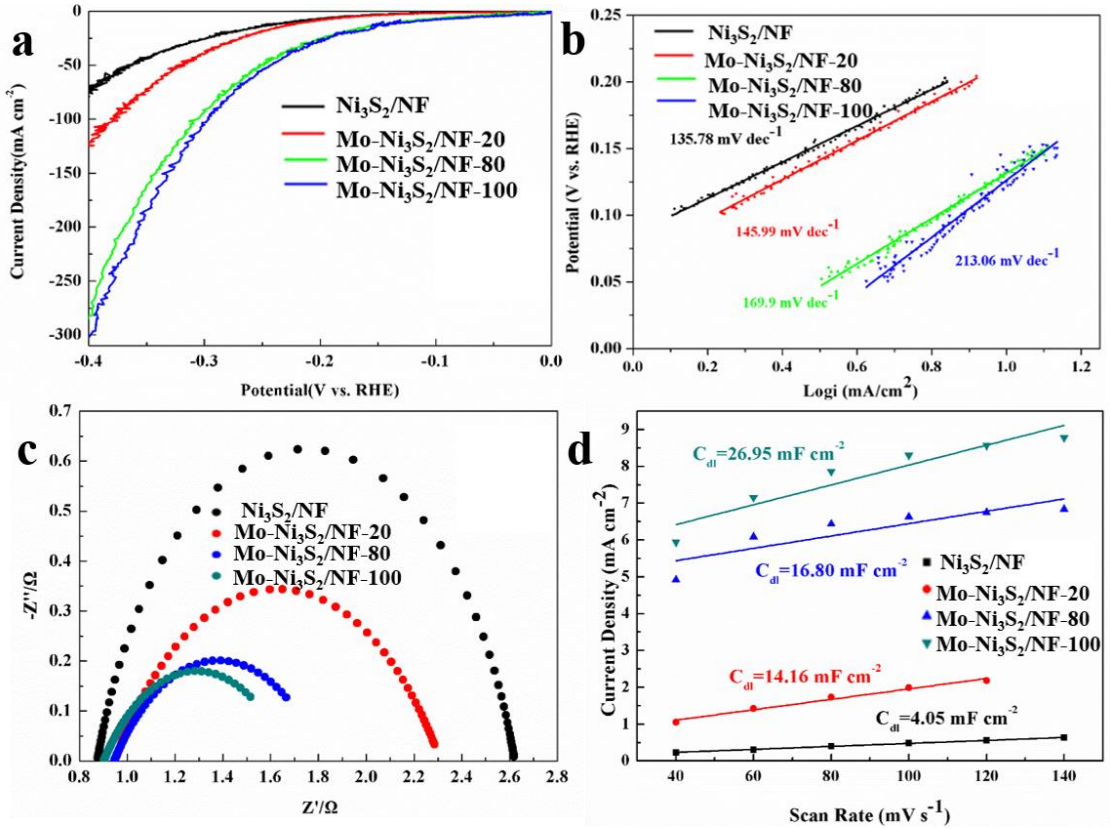

Figure 5. (a) Comparison of LSV curves on Ni_3S_2/NF, Mo-Ni_3S_2/NF-20, Mo-Ni_3S_2/NF-80 and Mo-Ni_3S_2/NF-100 for HER. (b) Corresponding Tafel plots extracted from panel a. (c) Nyquist plots of Ni_3S_2/NF, Mo-Ni_3S_2/NF-20, Mo-Ni_3S_2/NF-80 and Mo-Ni_3S_2/NF-100 at -0.1 V (vs. RHE) from 10^5 to 0.1 Hz. (d) C_{dl} values of Ni_3S_2/NF, Mo-Ni_3S_2/NF-20, Mo-Ni_3S_2/NF-80 and Mo-Ni_3S_2/NF-100.

Inspired by the above results, an alkaline electrolyzer was constructed with Mo-Ni_3S_2/NF-100 as bifunctional electrocatalyst to evaluate its activity for overall water splitting. As shown in Figure 6a, the Mo-Ni_3S_2/NF-100 couple catalyzed water splitting at 1.83 V with current density of 100 mA.cm^{-2}, outperforming other reported non-precious electrocatalysts (Table 1). Moreover, the Mo-Ni_3S_2/NF-100 couple based electrolyzer maintained favorable robustness, as demonstrated by the i-t curve (Figure 6b). Specifically, by applying a constant cell potential of 1.81 V, the catalytic current density maintains at around 60 mA.cm^{-2} for 10 h successive oxygen evolution. This result suggests that Mo-Ni_3S_2/NF-100 possesses excellent bifunctional catalytic activity and stability in 1 M KOH.

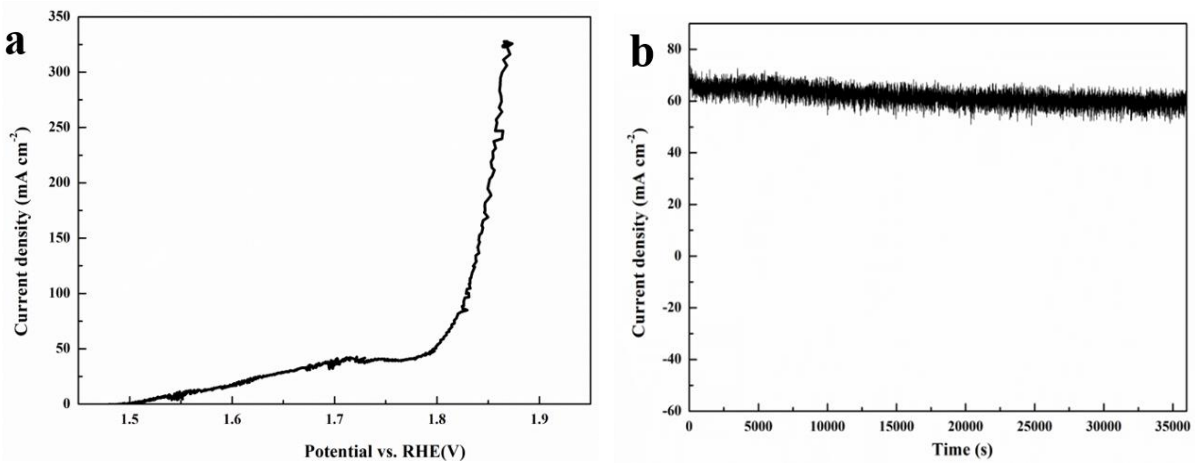

Figure 6. (a) Linear sweep voltammograms in 1M KOH for an electrolyzer whose anode and cathode both contain Mo-Ni_3S_2/NF-100 as electrocatalysts. (b) The corresponding current density versus time curves at a potential of 1.81 V.

Table 1 Comparisons of overall water splitting performances of Mo-Ni_3S_2/NF-100 with other non-precious catalysts in 1.0 M KOH.

Catalyst	***J* (mA cm^{-2})**	**Voltage (V)**	**Ref.**
Mo-Ni_3S_2/NF-100	**100**	**1.83**	**This work**
N, F doped graphene nanosheets	10	1.91	52
NiFeOF	10	1.83	53
N- Ni_3S_2/NF	100	1.85	54
NP	100	1.9	55

Such excellent electrocatalytic activity of Mo-Ni_3S_2/NF-100 for both HER and OER could be ascribed to the following reasons. (i) Its unique nanorod arrays with large specific surface area result in high accessibility of active sites and facilitate gas release and charge transfer. (ii) Nickle sulfides are considered as active electrocatalyst for HER and OER. Notably, when Nickle sulfides used as OER catalyst, the Nickle sulfides would partially transform to Nickle oxides, which are the true active sites for OER process. (iii) The doping of Mo into Nickle sulfides would improve electrocatalytic activity of electrocatalysts through synergistic effect between Nickle sulfides and Mo oxides. All these factors collectively benefit the catalytic performance of Mo-Ni_3S_2/NF-100 for water electrolysis.

4. CONLUSIONS

In summary, a simple molybdate-directed route to synthesize Mo doped Ni_3S_2 nanorod arrays for water electrolysis have been demonstrated. The Mo-Ni_3S_2/NF-100 heterogenous nanorod arrays, decorated with vertical nanosheets, possessed excellent catalytic performance toward both OER and HER, delivering current density of 100 $mA.cm^{-2}$ at overpotential of 350 and 290 mV, respectively. Moreover, the Mo-Ni_3S_2/NF-100 couple based alkaline electrolyzer could deliver a high current density of 100 $mA.cm^{-2}$ at a cell voltage of 1.83 V, along with remarkable durability.

ACKNOWLEDGEMENTS
This work is financially supported Shandong Provincial Natural Science Foundation of China (ZR2016BL22), the Fundamental Research Funds for the Central Universities (17CX02061), the Qingdao Applied Basic Research Project (17-1-1-73-jch) and the State Key Laboratory of Heavy Oil Processing (SLKZZ-2017005).

References

1. W. H. Hu, X. Shang, J. Xue, B. Dong, J. Q. Chi, G. Q. Han, Y. R. Liu, X. Li, K. L. Yan, Y. M. Chai, C. G. Liu, *Int. J. Hydrogen Energy*, 42 (2017) 2088.
2. X. X. Zou, Y. Zhang, *Chem. Soc. Rev.*, 44 (2015) 5148.
3. G. Han, Y. H. Jin, R. A. Burgess, N. E. Dickenson, X. M. Cao, Y. Sun, *J. Am. Chem. Soc.*, 139 (2017) 15584.
4. J. Q. Chi, W. K. Gao, J. H. Lin, B. Dong, J. F. Qin, Z. Z. Liu, B. Liu, Y. M. Chai, C. G. Liu, *J. Catal.*, 360 (2018) 9.
5. B. Dong, X. Zhao, G. Q. Han, X. Li, X. Shang, Y. R. Liu, W. H. Hu, Y. M. Chai, H. Zhao, C. G. Liu, *J. Mater. Chem. A*, 4 (2016) 13499.
6. K. L. Yan, J. F. Qin, Z. Z. Liu, B. Dong, J. Q. Chi, W. K. Gao, J. H. Lin, Y. M. Chai, C. G. Liu, *Chem. Eng. J.*, 334 (2018) 922.
7. X. Shang, K. L. Yan, Y. Rao, B. Dong, J. Q. Chi, Y. R. Liu, X. Li, Y. M. Chai, C. G. Liu, *Nanoscale*, 9 (2017)12353.
8. X. Li, G. Q. Han, Y. R. Liu, B. Dong, W. H. Hu, X. Shang, Y. M. Chai, C. G. Liu, *ACS Appl. Mater. Interfaces*, 8 (2016) 20057.
9. X. Shang, K. L. Yan, S. S. Lu, B. Dong, W. K. Gao, J. Q. Chi, Z. Z. Liu, Y. M. Chai, C. G. Liu, *J. Power Sources*, 363 (2017) 44.
10. L. L. Feng, G. Yu, Y. Wu, G. D. Li, H. Li, Y. Sun, T. Asefa, W. Chen, X. X. Zou, *J. Am. Chem. Soc.*, 137 (2015) 14023.
11. N. Jiang, B. You, M. Sheng, Y. Sun, *Angew. Chem., Int. Ed.*, 127 (2015) 6349.

12. J. Yin, P. P. Zhou, L. An, L. Huang, C. W. Shao, J. Wang, H. Y. Liu, P. X. Xi, *Nanoscale*, 8 (2016) 1390.
13. Z. Yin, Y. Sun, C. Zhu, C. Li, X. Zhang, Y. Chen, *J. Mater. Chem.* A, 5 (2017) 13648.
14. J. T. Zhang, L. M. Dai, *Angew. Chem. Int. Ed.,* 55 (2016) 13296.
15. G. Q. Han, Y. R. Liu, W. H. Hu, B. Dong, X. Li, X. Shang, Y. M. Chai, Y. Q. Liu, C. G. Liu, *Appl. Surf. Sci.*, 359 (2015) 172.
16. T. F. Jaramillo, K. P. Jorgensen, J. Bonde, J. H. Nielsen, S. Horch, I. I. Chorkendorff, *Science*, 317 (2007) 100.
17. J. Kibsgaard, Z. Chen, B. N. Reinecke, T. F. Jaramillo, *Nat. Mater.*, 11 (2012) 963.
18. Y. Li, H. Wang, L. Xie, Y. Liang, G. Hong, H. Dai, *J. Am. Chem. Soc.*, 133 (2011) 7296.
19. Y. Sun, C. Liu, D. C. Grauer, J. Yano, J. R. Long, P. Yang, C. J. Chang, *J. Am. Chem. Soc.*, 135 (2013) 17699.
20. B. You, N. Jiang, M. Sheng, Y. Sun, *Chem. Commun.*, 51 (2015) 4252.
21. H. B. Wu, B. Y. Xia, L. Yu, X. Y. Yu, X. W. Lou, *Nat. Commun.*, 6 (2015) 6512.
22. G. Q. Han, Y. R. Liu, W. H. Hu, B. Dong, Y. M. Chai, X. Li, X. Shang, Y. Q. Liu, C. G. Liu, *Journal of The Electrochemical Society*, 163 (2016) H67.
23. D. Kong, H. Wang, Z. Lu, Y. Cui, *J. Am. Chem. Soc.*, 136 (2014) 4897.
24. T. Y. Ma, S. Dai, M. Jaroniec, S. Z. Qiao, *J. Am. Chem. Soc.*, 136 (2014) 13925.
25. B. You, P. Yin, L. An, *Small*, 10 (2014) 4352.
26. J. G. Luo, J. H. Im, M. T. Mayer, M. Schreier, M. K. Nazeeruddin, N. G. Park, S. D. Tilley, H. J. Fan, M. Grätzel, *Science*, 345 (2014) 1593.
27. J. W. Miao, F. X. Xiao, H. B. Yang, S. Y. Khoo, J. Z. Chen, Z. X. Fan, Y. Y. Hsu, H. M. Chen, H. Zhang, B. Liu, *Sci. Adv.*, 1 (2015) e1500259.
28. X. D. Wang, Y. F. Xu, H. S. Rao, W. J. Xu, H. Y. Chen, W. X. Zhang, D. B. Kuang, C. Y. Su, *Energy Environ. Sci.*, 9 (2016) 1468.
29. X. D. Yan, K. X. Li, L. Lyu, F. Song, J. He, D. M. Niu, L. Liu, X. L. Hu, X. B. Chen, *ACS Appl. Mater. Interfaces*, 8 (2016) 3208.
30. X. Li, K.L. Yan, Y. Rao, B. Dong, X. Shang, G.Q. Han, J. Q. Chi, W. H. Hu, Y. R. Liu, Y. M. Chai, C. G. Liu, *Electrochimica Acta*, 220 (2016) 536.
31. M. R. Gao, J. X. Liang, Y. R. Zheng, Y. F. Xu, J. Jiang, Q. Gao, J. Li, S. H. Yu, *Nat. Commun.*, 6 (2015) 5982.
32. H. Lin, Z. Shi, S. He, X. Yu, S. Wang, Q. Gao, Y. Tang, *Chem. Sci.*, 7 (2016) 3399.
33. C. Ouyang, X. Wang, C. Wang, X. Zhang, J. Wu, Z. Ma, S. Dou, S. Wang, *Electrochim. Acta*, 174 (2015) 297.
34. L. L. Feng, G. Yu, Y. Wu, G. D. Li, H. Li, Y. Sun, T. Asefa, W. Chen, X. Zou, *J. Am. Chem. Soc.*, 137 (2015) 14023.
35. W. X. Zhu, X. Y. Yue, W. T. Zhang, S. X. Yu, Y. H. Zhang, J. Wang, J. L. Wang, *Chem. Commun.*, 52 (2016) 1486.
36. Y. Y. Wu, G. D. Li, Y. P. Liu, L. Yang, X. R. Lian, T. Asefa, X. X. Zou, *Adv. Funct. Mater.*, 26 (2016) 4839.
37. C. Tang, Z. Pu, Q. Liu, A. M. Asiri, Y. Luo, X. Sun, I*nt. J. Hydrogen Energy*, 40 (2015) 4727.
38. Y. Yang, K. Zhang, H. Lin, X. Li, H. C. Chan, L. Yang, Q. Gao, *ACS Catal.*, 7 (2017) 2357.
39. J. Zhang, T. Wang, D. Pohl, B. Rellinghaus, R. Dong, S. Liu, X. Zhuang, X. Feng, *Angew.Chem.Int. Ed.*, 55 (2016) 6702.
40. J. Wang, D. L. Chao, J. L. Liu, L. L. Li, L. F. Lai, J. Y. Lin, Z. X. Shen, *Nano Energy*, 7 (2014)151.
41. T. C. An, Y. Wang, J. Tang, W. Wei, X. Q. Cui, A. M. Alenizi, L. J. Zhang, G. F. Zheng, *J. Mater. Chem. A*, 4 (2016) 13439.
42. N. Jiang, Q. Tang, M. Sheng, B. You, D. E. Jiang, Y. Sun, *Catal. Sci. Technol.*, 6 (2016) 1077.
43. N. Liu, L. Yang, S. Wang, Z. Zhong, S. He, X. Yang, Q. Gao, Y. Tang, *J. Power Sources*, 275 (2015) 588.

44. N. Liu, Y. L. Guo, X. Y. Yang, H. L. Lin, L. C. Yang, Z. P. Shi, Z. W. Zhong, S. N. Wang, Y. Tang, Q. S. Gao, *ACS Appl. Mater. Interfaces*, 7 (2015) 23741.
45. Q. Gao, S. Wang, H. Fang, J. Weng, Y. Zhang, J. Mao, Y. J. Tang, *Mater. Chem.*, 22 (2012) 4709.
46. D. Guo, Y. Luo, X. Yu, Q. Li, T. Wang, *Nano Energy*, 8 (2014) 174.
47. Y. R. Liu, X. Shang, W. K. Gao, B. Dong, X. Li, X. H. Li, J. C. Zhao, Y. M. Chai, Y. Q. Liu, C. G. Liu, *J. Mater. Chem. A*, 5 (2017) 2885.
48. G. Q. Han, X. Li, J. Xue, B. Dong, X. Shang, W. H. Hu, Y. R. Liu, J. Q. Chi, K. L. Yan, Y. M. Chai, C. G. Liu, *Int. J. Hydrogen Energy*, 42 (2017) 2952.
49. K. L. Yan, X. Shang, L. M. Zhang, B. Dong, Z. Z. Liu, J. Q. Chi, W. K. Gao, Y. M. Chai, C. G. Liu, *Electrochimi. Acta*, 249 (2017) 16.
50. J. Q. Chi, X. Shang, F. Liang, B. Dong, X. Li, Y. R. Liu, K. L. Yan, W. K. Gao, Y. M. Chai, C. G. Liu, *Appl. Surf. Sci.*, 401 (2017) 17.
51. X. Shang, W. H. Hu, X. Li, B. Dong, Y. R. Liu, G. Q. Han, Y. M. Chai, C. G. Liu, *Electrochim. Acta*, 224 (2017) 25.
52. X. Yue, S. Huang, J. Cai, Y. Jin, P. K. Shen, *J. Mater. Chem. A*, 5 (2017) 7784.
53. K. Liang, L. Guo, K. Marcus, S. Zhang, Z. Yang, D. E. Perea, L. Zhou, Y. Du, Y. Yang, *ACS Catal.*, 7 (2017) 8406.
54. P. Chen, T. Zhou, M. Zhang, Y. Tong, C. Zhong, N. Zhang, L. Zhang, C. Wu, Y. Xie, *Adv. Mater.*, 29 (2017) 1701584.
55. R. Ding, S. Cui, J. Lin, Z. Sun, P. Du, C. Chen, *Catal. Sci. Technol.*, 7 (2017) 3056.